National Aeronautics and Space Administration

Orbital Debris Quarterly News

Volume 26, Issue 4
December 2022

Inside...

A publication of the NASA Orbital Debris Program Office (ODPO)

International Space Station Maneuvers to Avoid Another Russian ASAT Fragment

The International Space Station (ISS) conducted a second collision avoidance maneuver for the year at 19:25 CDT on Monday, 24 October 2022, to avoid a potential high-risk collision with a large debris fragment (International Designator 1982-092BMN, Catalog Number 51561). Object 51561 was generated as a result of the anti-satellite (ASAT) test on Cosmos 1408 by the Russian Federation on 15 November 2021 (ODQN, vol. 26, issue 1, March 2022, pp. 1-5). The previous ISS collision avoidance maneuver occurred in June 2022 (ODQN, vol. 26, issue 3, September 2022, pp. 1). That maneuver was performed to also avoid a Cosmos 1408 fragment (International Designator 1982-092BYX, Catalog Number 52590).

continued on page 2

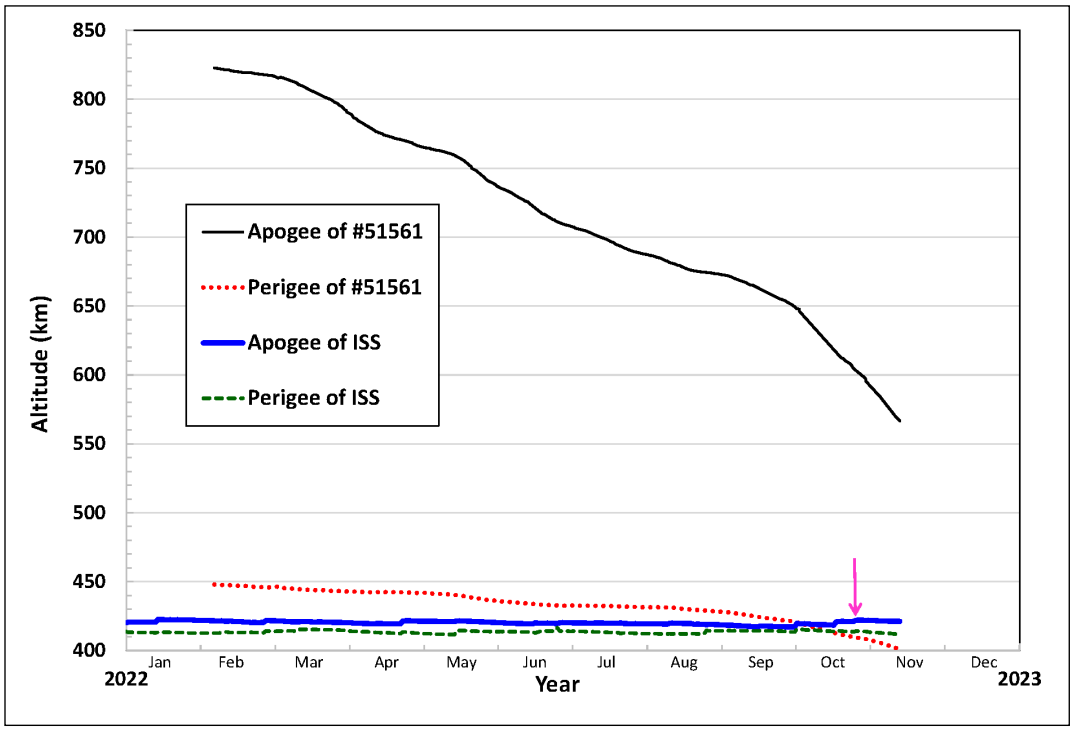

Figure 1. Apogee and perigee altitude history of Object 51561 and the ISS. The down arrow indicates when the latest ISS collision avoidance maneuver was conducted.

ISS Maneuvers

continued from page 1

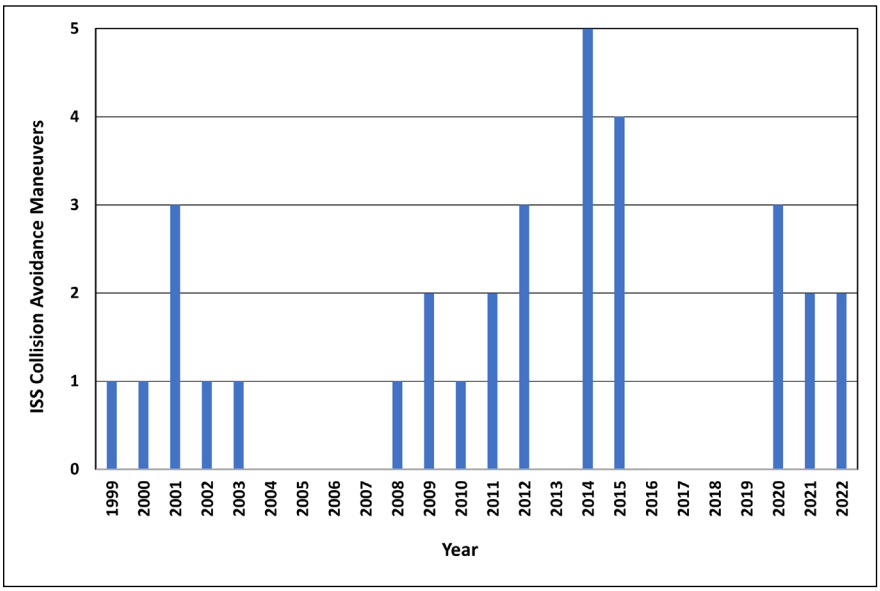

Figure 2. History of the ISS collision avoidance maneuvers.

The orbit of Cosmos 1408 prior to the ASAT test was 490 × 465 km altitude, but many of the resulting fragments, including Object 51561, were ejected into orbits with apogee altitudes significantly higher than 490 km (ODQN, vol. 26, issue 1, March 2022, pp. 1-5). As those fragments decay due to atmospheric drag, their orbits eventually intersect that of the ISS, making conjunctions possible.

Figure 1 shows the apogee and perigee altitudes of Object 51561 and the ISS. The maneuver on 24 October 2022 raised the apogee and perigee altitudes of the ISS by approximately 0.4 km and 1.3 km, respectively, an adjustment deemed sufficient to mitigate the risk of a collision.

The ISS has experienced many conjunctions with the large, tracked Cosmos 1408 fragments since the ASAT test. This latest collision avoidance maneuver was the second time a maneuver was necessary to avoid fragments from the Cosmos 1408 event. The number of ISS collision avoidance maneuvers against objects large enough to be tracked since 1999 has now reached a total of 32 (Figure 2). ♦

PROJECT REVIEW

DebriSat Analysis and Shape Categorization

H. COWARDIN, J. MURRAY, J. SEAGO, A. MANIS, AND J. OPIELA

The DebriSat project continues to assess the multitude of fragments generated from the 2014 hypervelocity impact test at the Air Force Arnold Engineering Development Complex. As a collaboration between the NASA Orbital Debris Program Office (ODPO), the Space Force Space Systems Command (formerly the Air Force Space and Missile Systems Center), The Aerospace Corporation, and the University of Florida, the stakeholders continue to refine the critical measurements needed to update breakup and environmental models. The original goals for the project were 1) to design and fabricate a 56-kg-class spacecraft ("DebriSat") representative of modern spacecraft in the low Earth orbit environment; 2) to conduct a hypervelocity laboratory impact test to simulate a catastrophic fragmentation event of DebriSat; 3) to collect, measure, and characterize all fragments down to 2 mm in size; and 4) to use the data to improve space situational awareness applications and satellite breakup models for better orbital debris environment definition. The data from DebriSat, in addition to prior laboratory experimental tests such as the Satellite Orbital Debris Characterization Impact Test (SOCIT) and on-orbit events, will play a key role in updates to the NASA Orbital Debris Engineering Model (ORDEM). The ODPO continues to assess the evolving fragment distributions to assess a new parameter to be implemented – shape – and the relationship to material density and size to better characterize risk to objects in Earth orbit.

DebriSat database updates are provided by the University of Florida to the project's stakeholders on a quarterly basis. These regular deliverables allow for further analysis and for stakeholders to determine if the priorities for fragment characterization need to be reassessed for a dynamic dataset. Recently, the team focused on characterizing fragments larger than 10 mm to mitigate the overwhelming contribution of small needle-like fragments generated from carbon fiber reinforced polymers (CFRP) as was shown in (ODQN, vol. 25, issue 2, June 2021, pp. 7-10). To date, the project continues to fully characterize fragments 10 mm and larger and increase the verification of recorded fragments in the database. The number of larger fragments has continued to increase in recent database updates; for example, the number of fragments with a characteristic length (L_c) greater than 10 mm increased by 43% from the February 2022 version of the database to the October 2022 version.

Figure 1 shows the cumulative number of fragments as a function of L_c for the most dominant materials in the DebriSat database. Although some fragments may be associated with more than one material, the primary (dominant) material is used for assigning each fragment's material. As discussed in (ODQN, vol. 25, issue 2, June 2021, pp. 7-10), the NASA Standard Satellite Breakup Model (SSBM) was formulated using data from laboratory tests, primarily from SOCIT, and ground-based remote measurements of on-orbit fragmentation events to provide an

continued on page 3

DebriSat Analysis

continued from page 2

average breakup ensemble for spacecraft and upper stage collisions and explosions [1]. Figure 1 includes the SSBM prediction for the cumulative number of fragments as a function of L_c from DebriSat, scaled by the total mass of collected fragments that have a corresponding L_c. The CFRP fragments continue to dominate the material categories for objects smaller than 15 mm. The second most dominant material is "Metal," a material category that includes aluminum, titanium, or stainless steel. Metal is noted in a generic nature as these materials are more difficult to identify purely on inspection until the full characterization and verification process is complete. There are two transitions of interest: one near 5 mm, where metal fragments become prominent over copper, plastic, and epoxy, and a second transition near 15 mm, where metal dominates all material categories.

Understanding the primary material distributions also provides insight into the shapes most likely to be associated with various materials/density categories. For example, it is well known based on the DebriSat analysis, that CFRP will tend to fragment into plate-like or needle/straight rod shape categories. As presented in Figure 2, the flat plate category is the most significant category until approximately 17 mm, where nuggets dominate the shape distribution for larger fragments. This is consistent with the material categories and transitions noted above. Between 1 mm and 4 mm, the straight rods, nuggets, and bent rods are all in close proximity in cumulative count. Near 7 mm, the bent plates become one of the top three shape categories (nugget, bent plate, and flat plates) for objects larger than 15 mm.

To further enhance the focus on shape distributions in order to improve updates to orbital debris models and assess the risk from shape, the team investigated binning these six primary shape categories into length-to-diameter ratios to simplify the categorizations into right-circular-cylinders (RCC). Utilizing RCC in terms of length to diameter allows for better integration with simulation and ground-based hypervelocity impact testing. The RCC approach scales the length (L) and diameter (D) of an RCC having the same volume as each fragment.

The RCC approach uses ellipsoidal-cylinder dimensions W_1, W_2, W_3 representing length, the semi-major axis, and the semi-minor axis, respectively. Table 1 provides the expressions used to translate ellipsoidal-cylinder dimensions into an RCC representation using length to diameter ratios for non-bent shapes; the equations are defined so that flattened fragments appearing like "flakes" or "plates" provide length-to-diameter ratios that are less than unity (1 to 1), so that length L represents a thickness, as a coin. Narrow, elongated pieces, such as needles or wires, have length-to-diameter ratios greater than unity, such that length L represents the longest dimension or length. Thereby, the length-to-diameter ratio of the virtual cylinder offers a single metric that correlates with the physical shape and size of the fragment.

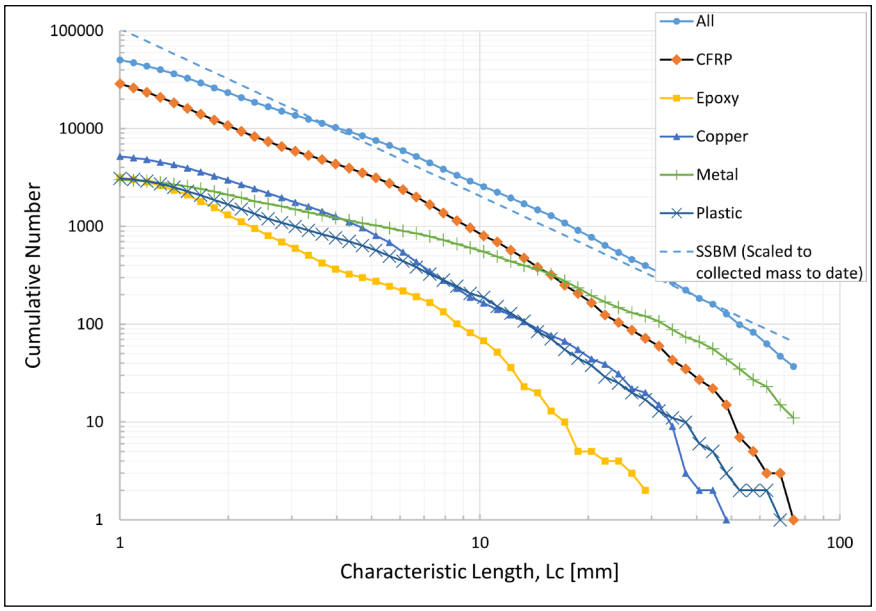

Figure 1. Cumulative number as function of L_c for prominent material categories, as of 06 October 2022.

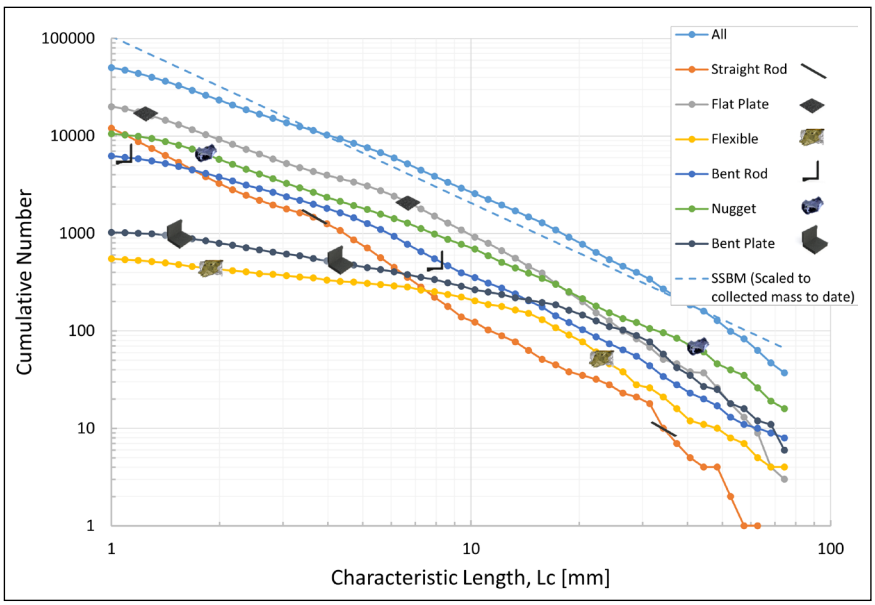

Figure 2. Cumulative number as a function of L_c for the six shape categories, as of 06 October 2022.

continued on page 4

DebriSat Analysis

continued from page 3

Table 1. Expressions Translating Cylindrical Dimensions ($W_1 > W_2 > W_3$) and Fragment Volume V into Right-Circular-Cylinder Length-to-Diameter Ratios

Virtual RCC Dimensions	Flat Plate/ Flake/Flexible	Nugget/ Spheroid/ Parallelepiped	Straight Rod/ Needle/Cylinder
L	$\frac{4\,V}{\pi\,W_1\,W_2}$	W_2	W_1
D	$\sqrt{W_1\,W_2}$	$\sqrt{\frac{4\,V}{\pi\,W_2}}$	$\sqrt{\frac{4\,V}{\pi\,W_1}}$
L:D	$\frac{4\,V}{\pi}(W_1\,W_2)^{-\frac{3}{2}}$	$\sqrt{\frac{\pi\,W_2^3}{4\,V}}$	$\sqrt{\frac{\pi\,W_1^3}{4\,V}}$

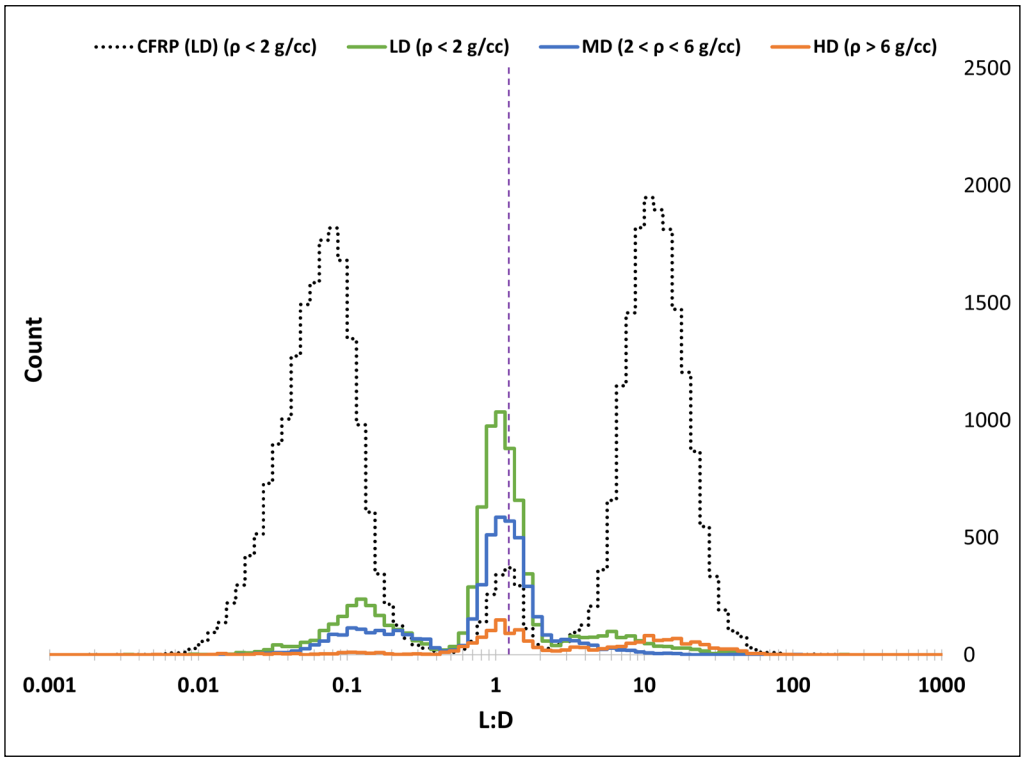

Figure 3. Histograms of right-circular-cylinder length-to-diameter ratios based on bulk volume ($V = V_{bulk}$). The vertical line references the RCC length-to-diameter value of a sphere. Peaks to the left, center, and right correspond to plates, nuggets, and rods, respectively.

Two formulations of volume are possible for fragments in the database: bulk volume, V_{bulk}, which accounts for partial voids and nonhomogeneous materials, and mass divided by material density, m/ρ. The use of V_{bulk} is presented in this preliminary research, as material density requires an assumption of an unambiguous material categorization. The generic category Metal makes utilization of material density for the RCC conversion unfeasible, and many DebriSat fragments are not homogenous in nature, thus the use of the parameter V_{bulk} reported in the DebriSat database. Assessing the DebriSat data by these three RCC shape categories yields a multimodal distribution shown in Figure 3 for four density categories. The far left corresponds to plate-like shapes with CFRP dominating, followed by low-density (LD) and medium-density (MD) material distributions. The length-to-diameter ratio distribution of CFRP is distinguished from other LD materials due to the fragmentation modes of CFRP. On the far right, the count of CFRP objects that fall into rod categories dominates LD, MD, and high-density (HD) fragments. These results are consistent with the CFRP and Metal category distributions discussed previously. The third histogram peak centered near length to diameter of 1 is consistent with spheres or "nuggets." In this region, non-CFRP LD dominates the shape distribution when RCC shapes are evaluated; only a small fraction of CFRP fragments is present near length-to-diameter ratio of 1 relative to the amount of CFRP rods and plates. The amount of HD rods from copper wiring is underrepresented in Figure 3 using only unbent samples.

To continue to provide updates for NASA's empirical orbital debris environmental and breakup models, such as ORDEM and the SSBM, the ODPO relies on the most recent validated datasets from various measurement sources, both laboratory and environmental. The data provided by DebriSat thus far has provided invaluable insight into the fragmentation of modern-day spacecraft, by means of the characterization of fragments, parameters associated with the DebriSat fragment total, and defining a key parameter (shape) needed for updating the models and tools used by the space community. As of this publication, the number of collected fragments of all sizes is estimated to exceed 227,000, a factor nearly three times higher than the original SSBM estimate of 85,000 fragments greater than 2 mm. The goal of the project continues to focus on characterizing the fragments in a timely manner, without bias and with verified information, such that updates to key models used by the space community can be provided in the near future.

Reference

1. Johnson, N., *et al.* "NASA'S NEW BREAKUP MODEL OF EVOLVE 4.0," Advances in Space Research, vol. 28, issue 9, pp. 1377-1384, (2001). ♦

PROJECT REVIEW

The Influence of Fragmentations and Mission-related Objects on the Space Environment

P. ANZ-MEADOR

NASA's Orbital Debris Program Office (ODPO) defines fragmentation debris as comprising breakup debris and anomalous debris [1]. Whereas the former is associated with energetic breakup events, the latter is generally a result of low-energy debris release events, sometimes called "shedding events." The catalog of breakup events is considered essentially complete for events in low Earth orbit (LEO) as the ODPO regularly coordinates with Department of Defense (DOD) colleagues; for that reason, this project review places more emphasis on breakup events. This article also summarizes the findings of a recent examination of a newly implemented category of mission-related objects (MROs), composed of mission-related debris (MRD) and other payload mission-related objects (*e.g.*, dispensed payloads) released during operations. Examples of MROs that do not fall in the MRD category would include the West Ford needles. The reference epoch for all data presented here is 01 May 2022.

The contribution of satellite fragmentations to the growth of the resident space objects (RSOs) is complex and varied. A slight majority of all cataloged fragmentation debris have already reentered the Earth's atmosphere, and the debris clouds from 38% of the 268 known, unique breakups have completely decayed. Moreover, just 10 of the 5820 space missions flown since 1957 are responsible for approximately 28% of all cataloged RSOs presently in orbit.

Table 1 presents two equally valid interpretations of the "Top 10" breakup event catalog. On the left side, the Top 10 is ordered in descending order by total debris cataloged. On the right side, the Top 10 is ordered by debris on orbit as of the reference epoch of 01 May 2022. Treat the left side as indicative of immediate consequence – and hence risk – after the event (noting that cataloging can take years or decades) and the right side as representing the long-term consequence. An example is provided by the STEP II rocket body (R/B), the Hydrazine Auxiliary Propulsion System upper stage of the Pegasus launch vehicle; this event, which was the largest to date when it occurred, required the accommodation of three-character piece tags in the international designator field for the first time, yet today is considered a relatively minor debris cloud. The top two events to produce a significant amount of fragmentation debris were the products of direct-ascent anti-satellite (ASAT) tests: 2009's *Fengyun-1C* (FY-1C) event and the 15 November 2021 catastrophic impact test with the derelict Cosmos 1408 spacecraft. Another ASAT test that occurred in 2019, conducted on the Microsat-R spacecraft by an Indian ASAT vehicle, resulted in a smaller cloud of cataloged debris due to its low perigee altitude and does not show up in the Top 10.

Relative to long-term risk, as presented on the table's right side, the sources of 3 of these 10 fragmentations were discarded R/Bs or separated fuel tanks that had operated as designed, but later broke up. Modern debris mitigation best practices such as passivation may have prevented these three events. The remaining seven fragmentations are diverse in character. The oldest to date is the fragmentation of Cosmos 1275, which Russian authorities report was caused by a battery fragmentation. Two fragmentation events, USA 109 and NOAA 16, share a similar spacecraft bus, and may share a root cause (ODQN, vol. 25, no. 4, December 2021, pp. 5-7). Again, modern design and debris mitigation best practices may have prevented these three events. More recently, the intentional FY-1C and Cosmos 1408 ASAT tests and the first accidental collision of large intact spacecraft, Cosmos 2251 and Iridium 33, account for about 21% of all cataloged RSOs on-orbit. The breakup fragments associated with these four spacecraft account for almost 15% of all objects cataloged since the launch of Sputnik 1 on 04 October 1957.

continued on page 6

Table 1. Breakup Event Sorts by Objects Cataloged and In-orbit at the Reference Epoch of 01 May 2022

Sort by Debris Cataloged				Sort by Debris On-orbit			
International Designator	Common Name	Debris Cataloged	Debris On-orbit	International Designator	Common Name	Debris Cataloged	Debris On-orbit
1999-025A	FENGYUN 1C	3532	2837	1999-025A	FENGYUN 1C	3532	2837
1982-092A	COSMOS 1408	1760	990	1993-036A	COSMOS 2251	1714	1064
1993-036A	COSMOS 2251	1714	1064	1982-092A	COSMOS 1408	1760	990
1994-029B	STEP II R/B	754	78	2000-055A	NOAA 16	458	457
1997-051C	IRIDIUM 33	657	330	1981-053A	COSMOS 1275	479	418
2006-026A	COSMOS 2421	509	0	1997-051C	IRIDIUM 33	657	330
1986-019C	SPOT 1 R/B	498	30	1970-025C	NIMBUS 4 R/B	442	297
1981-053A	COSMOS 1275	479	418	2011-037B	SL-23 DEBRIS	334	282
1965-082DM	OV2-1/LCS 2 R/B	473	32	1975-052B	NIMBUS 6 R/B	308	231
2000-055A	NOAA 16	458	457	1995-015A	USA 109 (DMSP 5D-2 F13)	238	212

Space Environment

continued from page 5

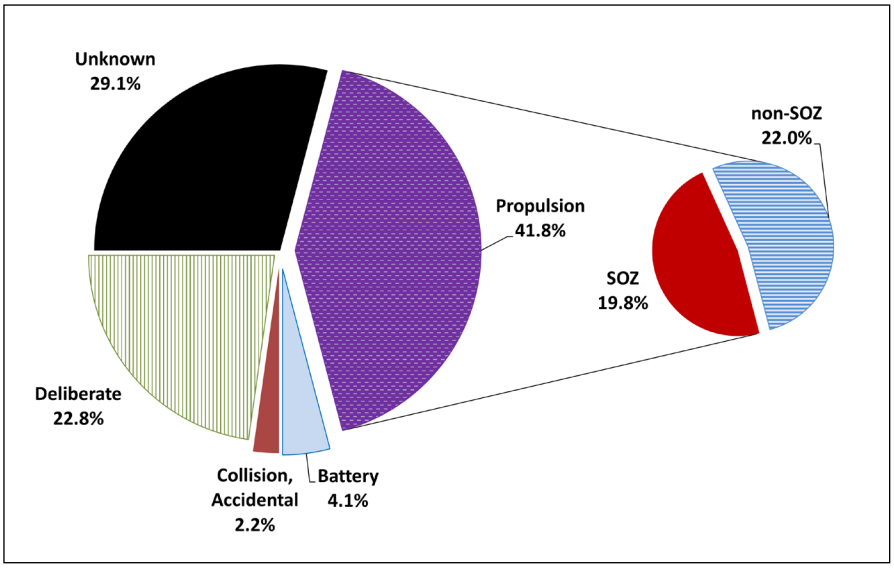

Figure 1. Causes of known satellite breakups.

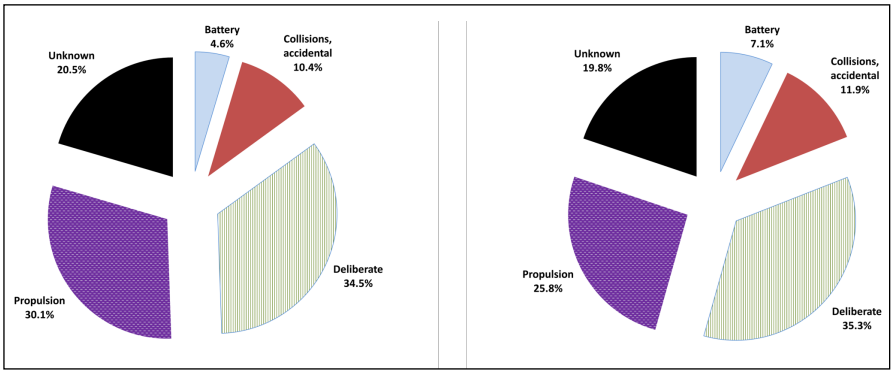

Figure 2. (left) Proportion of all cataloged satellite breakup debris; (right) proportion of cataloged satellite breakup debris remaining in orbit as of 01 May 2022.

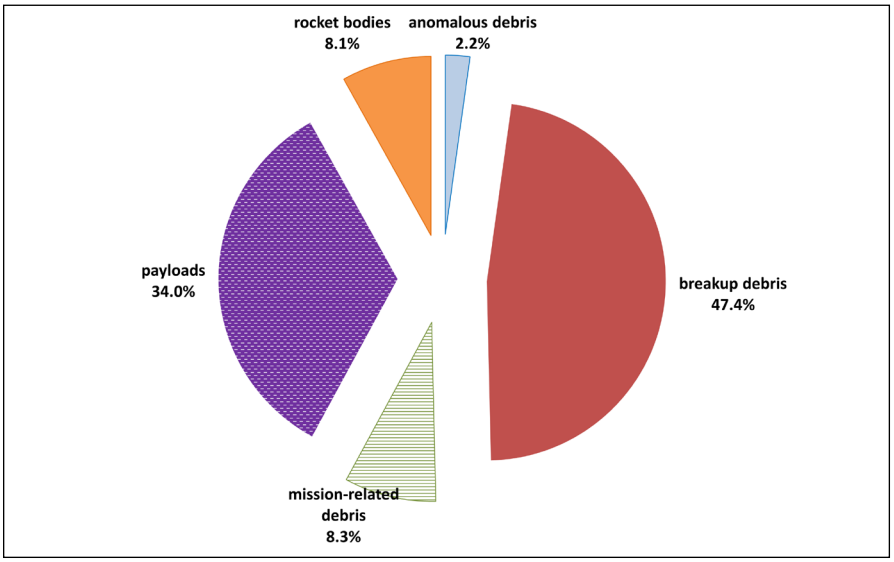

Figure 3. On-orbit population proportions at the reference epoch.

The primary known causes of satellite breakups, illustrated in Figure 1, are propulsion-related events and deliberate actions, although the cause for almost 30% of breakups remains uncertain. The ODPO will continue to carry breakup causes as unknown until a strong case can be made for one of the other root cause classifications.

Propulsion-related breakups, currently the most frequent class, include catastrophic malfunctions during orbital injection or maneuvers, subsequent explosions based on residual propellants, and failures of active attitude control systems. Breakups of R/Bs due to propulsion failures usually produce a larger number of longer-lived debris than the intentional destruction of payloads, often due to the higher altitudes of the malfunctioning R/Bs rather than the mechanics of the explosive event. Breakups of the Russian Blok-DM *Sistema Obespecheniya Zapuska* (SOZ) ullage motors are segregated from other members of the propulsion ensemble due to their high probability of fragmentation, which tends to overinflate the propulsion category to some degree; omitting the SOZ breakups roughly equates the non-SOZ propulsion and deliberate categories.

Deliberate actions were the most frequently occurring historical category through 1996's intentional fragmentation of Cosmos 2423, the final member of Cosmos 2031 class spacecraft, hence their persistence as a major category. This category was in near abeyance over the decade spanning 1997 to 2006, prior to 2007's FY-1C ASAT test.

Figure 2 compares cataloged and in-orbit proportions of breakup debris by root cause. The proportions of the latter plot directly reflect the influence of the initial orbit and specifics of the event, the debris physical attributes (area-to-mass ratio or ballistic coefficient, reflectivity, *etc.*), and subsequent solar activity and other space-related effects.

The relative proportion of fragmentation debris (breakup and anomalous debris) to the other generally recognized components of the orbital environment – payloads, R/Bs, and MRD – is shown in Figure 3 at the reference epoch. Nearly 50% of all objects on orbit are fragmentation debris.

The ODPO has recently conducted a study of objects in the MRD category from the perspectives of production frequency by spacecraft or R/Bs; production by R/B family; and the size or area of

continued on page 7

Space Environment

continued from page 6

sub-classes of MRD. The study is complicated by, among other factors, the historically low interest level afforded these objects; however, a detailed analysis in specific cases has revealed the presence of small numbers of the other population components. This is in some cases indicative of 1) catalog naming convention improvements and identification of actual objects in lieu of generic names such as "OBJECT A" and 2) launches examined in a manner only possible over long durations.

The results of this study are depicted in Figure 4. Here, spacecraft-related MRD are considered to be those objects either necessary for a separated spacecraft to function, such as lens or radiator covers, or those clearly dispensed by the spacecraft. In the left-hand image of Figure 4, "agnostic" debris are those not previously identified as related to either the spacecraft or rocket body sources, while the right-hand image makes those associations identified by the ODPO, as well as identifying non-MRD categories.

The proportions of debris associated with either spacecraft or R/B is essentially equal. Most of the spacecraft category are dispensed payloads, specifically the West Ford needles. For historical objects identified tentatively by the ODPO as fragmentation debris, Figure 5 shows a further breakdown by type. All fragmentation debris identified as such are distributed over multiple, small production events, *i.e.*, no one single event is responsible for the 164 explosion fragments. This work continues in an effort to better identify historical objects and trends and will be reflected in future editions of the ODQN (*e.g.*, the time series object type and mass charts presented annually).

It is worthwhile to consider sub-classes of MROs to better understand the presence of particular objects. For example, dual payload launches may employ payload encapsulation systems (PES) as exemplified by the Arianespace *Système de Lancement Double Ariane* (SYLDA) while multiple payload launches may employ significant payload support and dispensing structures, referred to as aerospace support equipment. Other launch vehicles may employ separable components, including fuel tanks, essential to their intended function.

As characterization of R/B MRD is considered more complete by sub-class at the time of writing, this MRD component over time can be examined to observe trends. This time series by sub-class for R/B MRD identifications to date is presented in Figure 6. In this figure, the introduction and on-going use of launchers employing PES and other relatively large MRD is clear, as are the presence of separated propellant tanks. Of note, the "SL-23 DEB" presented in Table 1 also used a separated fuel tank, previously discussed as a breakup event parent (ODQN, vol. 20, issues 1-2, January/April 2016, pp. 2-3; ODQN, vol. 24, issue 3, August 2020, pp. 2-3). Work remains to further identify and distribute generic MRD by sub-class.

In this project review, the current state of the fragmentation debris environment has been presented, along with the effort to better characterize MROs. The intentional nature of the top two most prolific breakup events does not diminish, to any degree, the imperative for launch providers and spacecraft or constellation

continued on page 8

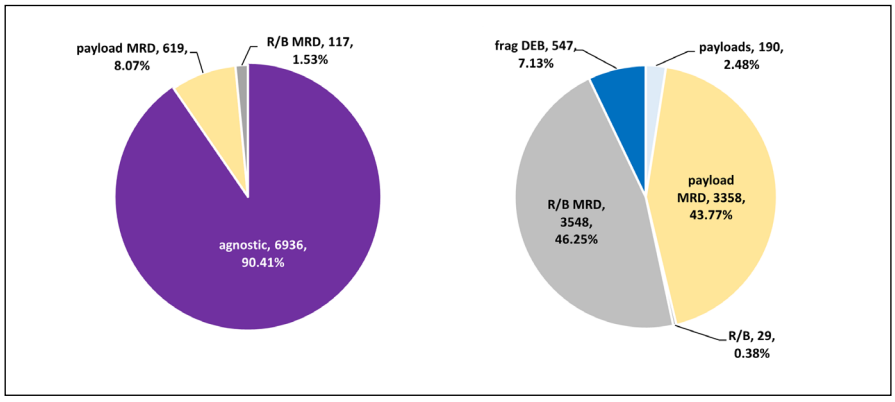

Figure 4. (left) A pre-study description of MRD in the ODPO database; (right) post-study in which the 7672 historical MRD are associated with their parent bodies or properly identified as belonging to the more general MROs or other population component categories.

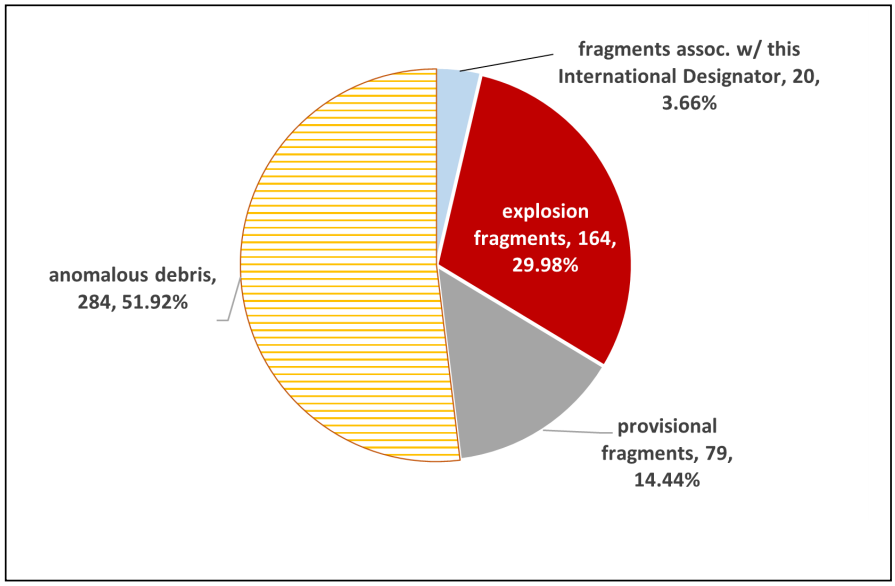

Figure 5. Fragmentation debris isolated in the MRD study. "Fragments associated with this International Designator" refer to cases where the parent object (spacecraft or R/B[s]) could not be determined. "Provisional fragments" refers to a historical debris ensemble whose particulars are not available.

Space Environment

continued from page 7

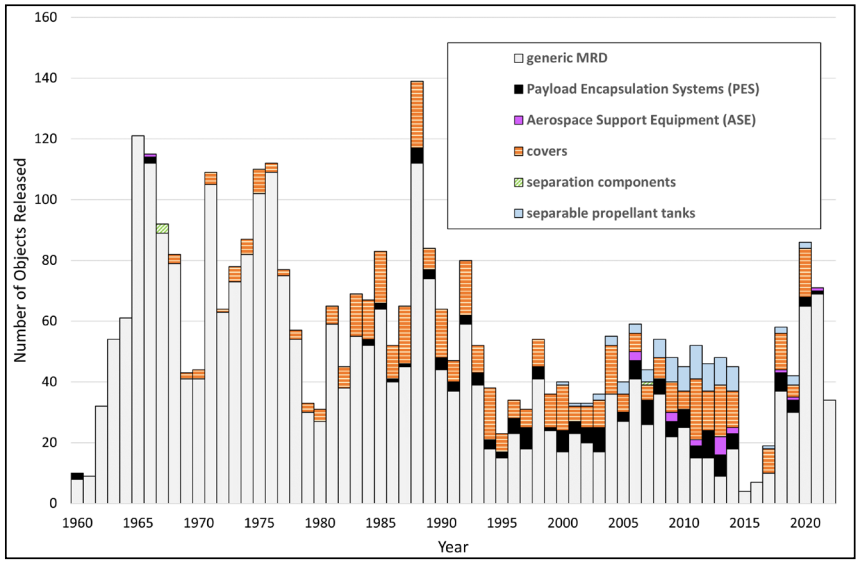

Figure 6. Rocket body MRD by sub-class.

owner/operators to continue employing best practices in their design and operations and adhering to existing domestic and international guidelines to mitigate the growth of orbital debris. As noted previously (ODQN, vol. 23, issues 1-2, May 2019, pp. 6-7), proactive design and operational procedures, when implemented, have proven their worth by demonstrably reducing fragmentations over multiple launch agencies and vehicle types.

Reference

1. Anz-Meador, P., *et al.* "History of On-orbit Satellite Fragmentations (15th edition)," NASA/TM-2018-220037. NASA Johnson Space Center, Houston, TX, USA, (2018). ♦

ABSTRACTS FROM THE NASA ORBITAL DEBRIS PROGRAM OFFICE

Meteoroids 2022, 13-17 June 2022, Virtual

An Analytic Formulation of Ejecta Distributions over Airless Bodies

M. MATNEY

With recent plans to revisit the Moon by robotic and crewed spacecraft, there has been a renewed interest in understanding the ejecta environment on the Moon and other airless bodies. Meteoroid and asteroid impacts can excavate large amounts of material from the surface and, above an airless body, can send this material long distances on (essentially) ballistic orbits. This ejecta, while typically traveling slower than the impactor, can nevertheless achieve high enough speeds to endanger surface operations. Accurate knowledge of this phenomenon is necessary in order to design appropriate shielding for human activities, both for activities on the surface of the Moon and for orbiters in near-lunar space.

This phenomenon is also important in the transport of particles above other Solar System objects, such as Jovian satellites, where this ejecta creates a kind of ever-present "halo" of particles around the gravitating body. While Monte Carlo techniques have been successfully used to model this environment, there are useful analytic expressions, developed for use in modeling the meteoroid environment, that can be used to describe this environment as well. Such analytic tools can shed light on the altitude, velocity, and directionality of these ejecta environments. ♦

NASA Thermal and Fluid Analysis Workshop (TFAWS), 06-09 September 2022, Virtual

Characterizing Char Rate and Extent in Fiber-Reinforced Plastics Using X-ray Computed Tomography

B. GREENE, C. OSTROM, AND S. ECKLEY

Orbital debris is a growing problem for the space industry and the world in general, and an important component of the problem is what happens when that debris reenters the Earth's atmosphere. With more spacecraft opting for fiber-reinforced polymer (FRP) components, we need to understand the thermal destruction process of these materials during an atmospheric reentry and how much of the material can survive to impact the ground. The NASA Orbital Debris Program Office (ODPO) has developed a new charring model for FRP components to be integrated into the latest version of the Object Reentry Survival Analysis Tool (ORSAT). To validate this new model, the ODPO performed several test series using the Inductively Coupled Plasma (ICP) Torch facility at UT Austin. To measure the extent of charred material at different conditions, some of the test samples were scanned using x-ray computed tomography (CT) by the Astromaterials Curation Lab at Johnson Space Center. 3D image analysis was then used to calculate the volume and density of the char in each test sample. This paper presents the image analysis methodology, an assessment of the accuracy of the data analysis, and a comparison with calculations using the ORSAT charring model. ♦

continued on page 9

ABSTRACTS - CONT.

Hypervelocity Impact Symposium (HVIS2022), 18-22 September 2022, Alexandria, Virginia

Updates on the DebriSat Hypervelocity Experiment and Characterization of Fragments in Support of Environmental Models

H. COWARDIN, C. CRUZ, J. MURRAY, J. SEAGO, A. MANIS, D. GATES, J. REYES, AND J. OPIELA

To develop, maintain, and update orbital debris environmental and break-up models, such as the NASA Orbital Debris Engineering Model (ORDEM) and the NASA Standard Satellite Breakup Model (SSBM), the NASA Orbital Debris Program Office (ODPO) relies on the most recent validated datasets from various measurement sources, both laboratory and environmental. One key project that will provide insight for break-up events using modern-day spacecraft materials and construction techniques is the DebriSat laboratory hypervelocity-impact test. Based on the mass of the target, the projectile, and the impact velocity, the expected number of fragments greater than 2 mm, generated using the NASA SSBM, was estimated to be close to 85,000. To date, the DebriSat fragment database continues to grow, with over 200,000 fragments collected that will help inform updates to the SSBM. Additionally, the growing fragment ensemble will support key parameters for the next release of NASA's environmental models, employing fragment shapes, densities, and size distributions.

To further support these environmental models, specifically the size parameter used in ground- based optical measurements, optical characterization on a subset of DebriSat fragments is being conducted in ODPO's Optical Measurement Center (OMC). Broadband bidirectional reflectance distribution (BRDF) measurements will provide insight into the optical-based NASA Size Estimation Model (OSEM). The OSEM equates an object's brightness to size (*e.g.*, diameter of a disk or sphere) given several assumed parameters, including a defined phase function, albedo, and range. To address the first defined parameter, the ODPO has been using raytracing software to simulate light conditions in the OMC and to generate phase functions (*i.e.*, specular, Lambertian, and experimentally derived) of known shapes, materials, and sizes.

This simulated data, in addition to the experimentally derived measurements collected in the OMC, will aid in determining whether a new phase function would be suitable for an updated OSEM. The OSEM also assumes a single-value albedo, thus pre-impact spectral measurements on a subset of DebriSat materials were acquired for baseline material characterization and to provide insight into spacecraft material taxonomies. This DebriSat spectral data, along with spectral measurements from other known spacecraft material samples, will allow for better analyses of albedo variations and the effect on size calculations of defined laboratory targets, thus further supporting OSEM updates.

This paper provides an overview of DebriSat, the status of the project, updates on the parameter distributions, an overview of the NASA SSBM, and ongoing fragment characterization efforts within the OMC. ♦

Analysis of Hypervelocity-Impacted Thin Films for Space Applications

M. WARD, P. ANZ-MEADOR, AND H. COWARDIN

Exposure to the harsh space environment and hypervelocity impacts from micrometeoroids and small orbital debris can affect space operations through long-term degradation of spacecraft materials, surfaces, or systems. Multi-layer insulation (MLI) and coated polyimide films are space- craft materials commonly found on the external surfaces of spacecraft for thermal control and protection. Characterizing the damage to these exposed materials with in-situ and laboratory measurements can better inform spacecraft designers and operators in understanding and mitigating surface or system degradation. In this paper, we examine flown Hubble Space Telescope (HST) Electronic Bay 5 MLI and coated, polyimide ground test articles to characterize hypervelocity impact damage. Impact feature cavities are inspected to identify damage, which can validate long-term degradation models, improve thermal management systems, or improve accuracy of damage predictions. An overview of the impact characterization using optical microscopy, narrow-band spectroscopy, and Scanning Election Microscopy/Energy Dispersive Xray (SEM/EDX) of the two materials is presented. Observations of robustness in the space environment, as well as a detailed assessment of cratering and penetration statistics for the spaceexposed sample, also are discussed. ♦

The 23rd Advanced Maui Optical and Space Surveillance Technologies Conference (AMOS), 27-30 September 2022, Maui, Hawaii

Spectral Characterization of Modern Spacecraft Materials

H. COWARDIN, J. REYES, E. PLIS, R. HOFFMANN, G. BADURA, J. SHAH, S. COLLMAN, M. BENGTSON, D. ENGELHART, AND T. SCOTT

One of the observational parameters of interest in ground-based optical measurements is ascertaining material properties using broadband filter photometry and spectroscopy for orbiting targets. Broadband photometry can provide reflectance measurements that can aid in producing color-color indices and assess if objects can be classified into families or taxonomies. However, these reflectance properties can vary due to aspect angle, phase angle, and general degradation of the target's exterior material. Spectral characterization can aid in material characterization utilizing known absorption bands and spectral signatures, but these signatures are affected by the same conditions described for remote observations. When utilizing ground-based measurements, it is well understood that material characterization

continued on page 10

ABSTRACTS - CONT.

continued from page 9

The 23rd Advanced Maui Optical and Space Surveillance Technologies Conference (AMOS), 27-30 September 2022, Maui, Hawaii - Cont.

Spectral Characterization - Cont.

is subject to variability due to space weathering and/or other external events (*i.e.*, collision or explosion). The focus of this study is on space weathering effects on spacecraft materials in low Earth orbit.

To better assess how materials are affected by the harsh space environment, specifically modern materials, a collection of materials were analyzed in both their pristine condition and after electron bombardment. This sample collection is part of an upcoming mission with the Materials International Space Station Experiment Flight Facility (MISSE-FF) that will be launched in 2022. These laboratory analyses on the samples will provide a ground-truth to compare with the *in situ* collected data. The data will also be stored in the NASA Johnson Space Center's Spacecraft Materials Spectral Database that is available to U.S. citizens and maintained by the Orbital Debris Program Office.

The following paper provides an overview of the materials investigated, laboratory, and database overview, and spectral results for both pristine and post-electron exposed conditions. The spectral signature data highlights which materials are stable, or remain relatively unchanged, and which materials vary significantly due to exposure and material configuration (variations due to rotation of the sample on a flat surface). Initial results on changes in spectral directional reflectance of the materials as a function of incident illumination direction are also presented. This data also will benefit the space situational awareness community with spectral characterization of novel materials that can support their respective optical measurements focused on material identification. ♦

Goniometric and Polarized Imaging Spectroscopic Lab Measurements of Spacecraft Material

C. LEE, C. BACHMANN P. SEITZER, AND H. COWARDIN

To better characterize the spectral response of common spacecraft materials, the following laboratory measurements are presented to support the Space Situational Awareness community in the analysis of remotely sensed observational data. Of interest is classifying material reflective properties using directional reflectance spectroscopy and spatially resolved polarized imaging spectroscopy, allowing laboratory data to be applicable to ground-based optical telescope observations. The team acquired a typical CubeSat solar panel and a sample of multi-layer insulation (MLI) commonly used on spacecraft for initial measurements. The directional spectral data were collected at the Goniometer of the Rochester Institute of Technology (GRIT) laboratory with a lab and field goniometer incorporating two Analytical Spectral Device (ASD) spectrometers, a small Labsphere integrating sphere also paired with an ASD spectrometer, and a Headwall micro-Hyperspec E-Series imaging spectrometer with an adjustable linear polarizer. The goniometer measures spectral bi-directional reflectance factor (BRF) data over a broad range from 350 – 2500 nm at 1 nm spacing with 3 nm spectral resolution in the visible and near infrared and 8 nm in the shortwave infrared. With the same spectral capabilities, the integrating sphere measures hemispherical-directional reflectance (HDR) in a 45°-nadir configuration. The Headwall imager covers a spectral range from 400 – 1000 nm with 1.6 nm spectral resolution. Our initial BRF measurements show interference effects for both materials typically observed with thin films and high infrared reflectivity. In contrast, the interference effects are not present in the HDR measurements of the MLI likely due to the interference effects being averaged out over the reflecting hemisphere. Spatially resolved polarization ratio maps show variability across the materials due to the varying surface structure. We outline a plan for expanding our analysis to a broader range of materials to characterize their directional reflectance spectroscopy. ♦

Observations of Small Debris from the Cosmos 1408 Anti-Satellite Test using the HUSIR and Goldstone Radars

J. MURRAY, C. OSTROM, T. KENNEDY, AND M. MATNEY

On 15 November 2021, Russia conducted a direct-ascent anti-satellite (ASAT) test against its Cosmos 1408 satellite, which had been in orbit since 1982. The test produced at least 1500 fragments trackable by the U.S. Space Surveillance Network (SSN). The test is a significant event because the resulting cloud has the potential to endanger the International Space Station and other satellites in low Earth orbit (LEO). For almost 30 years, the NASA Orbital Debris Program Office (ODPO) has used the Haystack Ultrawideband Satellite Imaging Radar (HUSIR), operated by the Massachusetts Institute of Technology's Lincoln Laboratory to perform statistical measurements of debris in LEO too small to be tracked by the SSN, nominally down to 5.5 mm at 1000 km altitude. The ODPO also utilizes the Goldstone Orbital Debris Radar (Goldstone), operated by NASA's Jet Propulsion Laboratory, to characterize the small debris environment in LEO down to approximately 3 mm at 1000 km altitude. To characterize the small debris component of the Cosmos 1408 ASAT test, a series of observation campaigns were conducted with the HUSIR and Goldstone radars. This paper discusses the observation planning, including beam overlap analysis needed for Goldstone bistatic operation, using a model of the debris cloud produced with the NASA Standard Satellite Breakup Model. A description of the radars and the data processing techniques used to analyze the data are also discussed. Finally, results of the measurement campaigns including cumulative count rate versus size and surface area flux versus altitude and inclination are presented. ♦

ABSTRACTS FROM THE NASA HYPERVELOCITY IMPACT TECHNOLOGY TEAM

Hypervelocity Impact Symposium (HVIS2022), 18-22 September 2022, Alexandria, Virginia

Development of Analysis Techniques for Non-Spherical Hypervelocity Impacts

J. MILLER, B. DAVIS, R. MCCANDLESS, A. DELGADO, D. HENDERSON, A. PARDO, D. RODRIGUEZ, AND M. SANDY

Advanced steps have been made to develop techniques to manufacture, accelerate to orbital speeds, and diagnose the orientation for projectiles representative of the collected debris from the DebriSat experiment. This model validation work has enabled the development of numerical models of metallic, Whipple shields. Using these developed numerical models, work has begun on developing ballistic performance corrections to existing ballistic-limit equations for future use in threat assessments with an environment definition that includes non-spherical orbital debris. As described here, a slightly decreased performance is expected for a specific Whipple shield; however, much is left to do for additional projectile fineness ratios and shield characteristics. ♦

Mapping and Measurement of Critical Damage to Complex Tubing Geometries in a Metallic Housing

R. MCCANDLESS, B. DAVIS, AND J. MILLER

A tangled web of titanium tubing inside a complex housing design creates a variety of challenges for hypervelocity impact testing and internal damage assessment. The Hypervelocity Impact Technology group (HVIT) at the NASA Johnson Space Center mapped potential internal damage by testing titanium tubing inside a simplified housing geometry. Innovative modeling and fabrication techniques allowed for a high-quality, low-cost assessment of the expected Hypervelocity Impact (HVI) performance of actual tube-containing structures. Thoughtful test-fixture design and analysis also allowed the impact testing of both a mass-reduced configuration and a worst-case scenario for MMOD shielding.

Using a simplified geometry allowed for a mirroring of damage where multiple configurations could be tested with identical criteria simultaneously. ♦

CONFERENCE AND WORKSHOP REPORTS

Thermal and Fluids Analysis Workshop, 06-09 September 2022, Virtual

The annual Thermal and Fluids Analysis Workshop was conducted virtually 06-09 September 2022. This event was sponsored by the NASA Engineering Safety Center and hosted by Kennedy Space Center. The workshop is a forum for keeping up to date on the latest advances and technologies for thermal and fluids analysis.

The keynote gave an overview of NASA's efforts to develop a Hypersonic Inflatable Aerodynamic Decelerator (HIAD); a flexible, deployable aeroshell for atmospheric reentry. The talk described the benefits of HIAD technology and outlined tests of various designs developed at NASA, ending with the upcoming flight test of the Low-Earth Orbit Flight Test of an Inflatable Decelerator (LOFTID) payload.

This year, the workshop hosted five session topics: aerothermal, cryothermal, passive thermal, active thermal/fluids/life support, and interdisciplinary. The NASA Orbital Debris Program Office presented recent work focused on validating the new Object Reentry Survival Analysis Tool (ORSAT) 7.0 charring model in the aerothermal session. This session also hosted papers on recent tests conducted in the NASA Langley Aerothermodynamic Laboratory, high fidelity reentry modeling, and recent advances in a variety of aerothermal computation codes.

Other paper sessions highlighted work on novel heat pipe designs, thermal design for lunar missions, passively deployed radiators, liquid nitrogen reaction control system design, and many others. In addition, several short courses were provided on grey bodies and radiation conductances, lunar thermal analysis best practices, passive cryogenic fluid management, reentry capsule computational fluid dynamics, and spaceflight instrument thermal design. ♦

The Hypervelocity Impact Symposium (HVIS2022), 18-22 September 2022, Alexandria, Virginia

The 16th Hypervelocity Impact Symposium (HVIS) was held in Alexandria, Virginia, on 18-22 September 2022. HVIS is a biennial event organized by the Hypervelocity Impact Society that serves as the principal forum to facilitate discussions and exchange information related to hypervelocity impact phenomenology.

This year's symposium was coordinated in conjunction with Johns Hopkins Applied Physics Laboratory and Missouri University of Science and Technology. The symposium attracted more than 170 attendees from government, industry, and academic organizations. Dr. Eric Christiansen of the NASA Hypervelocity Impact Technology (HVIT) team was presented the Distinguished Scientist Award and delivered the keynote address. Also presented were the Society's Best Paper Award and the Alex Charters Student Scholars Awards.

continued on page 12

REPORTS - CONT.

The Hypervelocity Impact Symposium - Cont.

This year's HVIS consisted of nine technical sessions and a poster session that covered hypervelocity penetration and target response; high-velocity launchers and diagnostics; hypervelocity phenomenology; material response; armor/anti-armor ballistic technology; state-of-the-art experiments enabling state-of-the-art models; asteroid impact and planetary defense; fracture and fragmentation; analytic and numerical methodologies; and spacecraft/meteoroid debris shielding and failure analysis.

From left to right, Josh Miller (HVIT/University of Texas at El Paso), Shannon Ryan (President of Hypervelocity Impact Symposium), and Dr. Eric Christiansen (Hypervelocity Impact and Orbital Debris Office Division Branch Chief) receiving the 2022 Distinguished Scientist Award. Credit: Johns Hopkins University/Applied Physics Laboratory.

A total of 49 oral and 14 poster papers were given, including NASA Orbital Debris Program Office (ODPO) presentations "Updates on the DebriSat Hypervelocity Impact Experiment and Characterization of Fragments in Support of Environmental Models," and "Analysis of Hypervelocity-impacted Thin Films for Space Applications." The NASA HVIT team presented "Mapping and Measurement of Critical Damage to Internal Components of the Reaction Control System Thrusters for Orion" and "Development of Experimental Techniques for Non-Spherical Hypervelocity Impacts."

Abstracts submitted by the ODPO and HVIT are located in this issue. HVIS will reconvene in September 2024. ♦

The 23rd Advanced Maui Optical and Space Surveillance Technologies Conference (AMOS), 27-30 September 2022, Maui, Hawaii

The 23rd Advanced Maui Optical and Space Surveillance Technologies Conference was held in hybrid format 27-30 September 2022. This year's record-breaking event hosted 1212 in-person attendees and 259 virtual participants, including representatives from 23 countries. Three keynote addresses were held this year, each followed by invited talks.

This year, 6 virtual short courses and 10 additional in-person short courses were provided at the start of the conference. The Space Debris session, co-chaired by representatives from NASA's Orbital Debris Program Office (ODPO), Purdue University, and Astronomisches Institut Universität Bern, focused on several themes. These included the current environment and all aspects of debris risks in LEO; analysis, modeling, and collision risk associated with the 2021 Cosmos 1408 event; evolution of debris clouds in low lunar orbit; identification of fragmentation epoch from surveillance radar observation; evaluation of collision potential in orbital shells; high-fidelity propagation and visualization for large numbers of resident space objects; statistical collision risk in LEO; detection methods for statistical analysis of satellites and space debris in astronomical images; the relationship between ozone depletion and orbital debris; DebriSat data collection and procedures; active debris removal (ADR) and modeling small orbital debris remediation; and a memo on ADR for the space debris summit.

The ODPO virtually presented a poster paper titled "Observations of Small Debris from the Cosmos 1408 Anti-Satellite Test using the HUSIR and Goldstone Radars," and in-person, a paper, "Spectral Characterization of Modern Spacecraft Materials," and a poster paper "Goniometric and Polarized Imaging Spectroscopic Lab Measurements of Spacecraft Materials."

Other presentations focused on Space Situational Awareness (SSA)/Space Domain Awareness (SDA); machine learning for SSA applications; SSA/SDA Technology policy; space-based assets; optical systems and instrumentation; astrodynamics, conjunctions and rendezvous proximity operations; atmospherics and space weather; and cislunar SSA.

The next AMOS conference is scheduled for 19-22 September 2023. ♦

SUBSCRIBE to the ODQN or UPDATE YOUR SUBSCRIPTION ADDRESS

To be notified when a new issue of the ODQN is published or to update your email address, subscribe on the NASA Orbital Debris Program Office (ODPO) website at: https://orbitaldebris.jsc.nasa.gov/quarterly-news/

UPCOMING MEETINGS

All information is current at the time of publication. Please consult the respective websites for updated schedule changes.

19-22 September 2023: 24th Advanced Maui Optical and Space Surveillance Technologies Conference, Maui, Hawaii, USA

The technical program of the 24th Advanced Maui Optical and Space Surveillance Technologies Conference (AMOS) will focus on subjects that are mission critical to space situational awareness. The technical sessions include papers and posters on orbital debris, space situational/space domain awareness, adaptive optics and imaging, astrodynamics, non-resolved object characterization, and related topics. The abstract submission deadline is 01 March 2023. Additional information about the conference is available at https://amostech.com.

02-06 October 2023: 74th International Astronautical Congress (IAC), Baku, Azerbaijan

The International Astronautical Congress (IAC) will convene in 2023 with a theme of "Global Challenges and Opportunities: Give Space a Chance." Of note, the 24th IAC was last held in Baku almost 50 years ago in 1973. The IAC's 21st International Academy of Astronautics Symposium on Space Debris will cover debris measurements and characterization; modeling; risk analysis; hypervelocity impact and protection; mitigation; post-mission disposal; space debris mitigation and removal; operations in the space debris environment; political and legal aspects of mitigation and removal; orbit determination and propagation; and financial gains with space debris. This year, the IAC will offer a venue for interactive presentations on space debris topics to allow more digital display capabilities for attendees. The abstract submission deadline is 28 February 2023. Additional information is available at https://www.iafastro.org/events/iac/iac-2023/ and http://iac2023.org/.

Save the Date for IOC II

Purpose and Scope

The goal of the 2nd International Orbital Debris Conference (IOC) is to promote orbital debris research activities in the United States and to foster collaborations with the international community. The 4-day conference will cover all aspects of meteoroid and orbital debris research, mission support, and other related activities.

Topics

- Measurements: radar, optical, *in situ*, laboratory, *etc.*
- Modeling: engineering, long-term environment, near-term risk assessments, reentry, *etc*.
- Operations and mission support: hypervelocity impact and protection, satellite anomalies, conjunction assessments, *etc*.
- Environment management: mitigation, remediation, space traffic coordination, policy, *etc*.

Important: To be added to the mailing list to receive additional information about this conference, submit an indication of interest by 01 May 2023.

https://www.hou.usra.edu/meetings/orbitaldebris2023/

SATELLITE BOX SCORE

(as of 04 November 2022, cataloged by the U.S. SPACE SURVEILLANCE NETWORK)

Country/ Organization	Spacecraft*	Spent Rocket Bodies & Other Cataloged Debris	Total
CHINA	597	3804	4401
CIS	1573	6164	7737
ESA	96	57	153
FRANCE	84	516	600
INDIA	106	111	217
JAPAN	206	112	318
UK	515	1	516
USA	5514	5196	10710
OTHER	1112	93	1205
TOTAL	9803	16054	25857

* active and defunct

Visit the NASA
Orbital Debris Program Office Website
www.orbitaldebris.jsc.nasa.gov

Technical Editor
Heather Cowardin, Ph.D.

Managing Editor
Ashley Johnson

Correspondence can be sent to:

Robert Margetta
robert.j.margetta@nasa.gov

or to:

Nilufar Ramji
nilufar.ramji@nasa.gov

National Aeronautics and Space Administration
Lyndon B. Johnson Space Center
2101 NASA Parkway
Houston, TX 77058

www.nasa.gov
https://orbitaldebris.jsc.nasa.gov/

Intl. = International; SC = Spacecraft; Alt. = Altitude; Incli. = Inclination; Addnl. = Additional; R/B = Rocket Bodies; Cat. = Cataloged
Notes: 1. Orbital elements are as of data cut-off date 30 September. 2. Additional spacecraft on a single launch may have different orbital elements. 3. Additional uncatalogued objects may be associated with a single launch.

INTERNATIONAL SPACE MISSIONS

01 July 2022 – 30 September 2022

Intl.* Designator	Spacecraft	Country/ Organization	Perigee Alt. (KM)	Apogee Alt. (KM)	Incli. (DEG)	Addnl. SC	Earth Orbital R/B	Other Cat. Debris
1998-067	ISS dispensed objects	Various	391	402	51.6	18	0	3
2022-073A	WFOV (USA 332)	US	35780	35795	0.3	0	1	1
2022-073B	USA 333	US	35339	35543	0.1			
2022-073E	USA 337	US	35540	35547	0.2			
2022-074A	RECURVE	US	488	493	45.0	5	0	0
2022-074C	OBJECT C	US	422	485	45.0			
2022-074E	OBJECT E	US	482	491	45.0			
2022-075A	COSMOS 2557 (GLONASS)	CIS	19098	19162	64.8	0	1	0
2022-076A	STARLINK-4260	US	539	541	53.2	52	0	4
2022-077A	STARLINK-4362	US	561	565	97.7	45	0	4
2022-078A	TIANLIAN-2 03	PRC	35785	35787	2.8	0	1	0
2022-079A	USA 334	US	623	633	40.0	0	2	0
2022-080A	LARES-2	IT	5882	5896	70.2	6	0	0
2022-080H	OBJECT H	TBD	5832	5854	70.1			
2022-081A	DRAGON CRS-25	US	193	382	51.6	0	0	1
2022-082A	SUPERVIEW NEO-2 O1	PRC	489	499	97.4	0	1	1
2022-082C	SUPERVIEW NEO-2 02	PRC	489	498	97.4			
2022-083A	STARLINK-4063	US	538	541	53.2	52	0	4
2022-084A	STARLINK-4391	US	561	565	97.7	45	0	4
2022-085A	CSS (WENTIAN)	PRC	380	387	41.5	0	1	0
2022-086A	STARLINK-4056	US	538	541	53.2	52	0	4
2022-087A	OBJECT A	PRC	490	509	97.4	0	1	0
2022-087B	OBJECT B	PRC	489	508	97.4			
2022-087C	OBJECT C	PRC	488	508	97.4			
2022-087D	OBJECT D	PRC	485	504	97.4			
2022-087E	OBJECT E	PRC	486	507	97.4			
2022-088A	YAOGAN-35 03A	PRC	493	501	35.0	0	1	1
2022-088C	YAOGAN-35 03B	PRC	495	498	35.0			
2022-088E	YAOGAN-35 03C	PRC	495	500	35.0			
2022-089A	COSMOS 2558	CIS	438	449	97.2	0	1	0
2022-090A	OBJECT A	PRC	500	507	97.5	0	1	0
2022-090B	OBJECT B	PRC	481	497	97.5			
2022-090C	OBJECT C	PRC	479	495	97.5			
2022-091A	USA 335	US	633	639	70.0	0	2	0
2022-092A	SBIRS-GEO 6 (USA 336)	US	35776	35800	6.4	0	1	0
2022-093A	PRC TEST SPACECRAFT2	PRC	597	608	50.0	0	1	6
2022-093J	OBJECT J	PRC	597	608	50.0			
2022-094A	KPLO	SKOR	EN ROUTE TO MOON			0	0	0
2022-095A	OBJECT A	PRC	434	541	97.4	0		
2022-095B	OBJECT B	PRC	434	540	97.4			
2022-095C	OBJECT C	PRC	435	542	97.4			
2022-095D	OBJECT D	PRC	428	543	97.4			
2022-096A	KHAYYAM	IRAN	490	492	97.4	16	0	0
2022-097A	STARLINK-4522	US	538	541	53.2	51	0	4
2022-098A	OBJECT A	PRC	530	545	97.5	15	0	0
2022-099A	STARLINK-4415	US	561	564	97.7	45	0	4
2022-100A	YAOGAN-35 04A	PRC	493	500	35.0	0	1	1
2022-100C	YAOGAN-35 04B	PRC	494	499	35.0			
2022-100E	YAOGAN-35 04C	PRC	494	499	35.0			
2022-101A	STARLINK-4511	US	539	541	53.2	52	0	4
2022-102A	CHUANG XIN 16A (CX-16A)	PRC	588	595	29.0	0	0	0
2022-102B	CHUANG XIN 16B (CX-16B)	PRC	588	595	29.0			
2022-103A	BEIJING 3B	PRC	595	617	97.9	0	0	0
2022-104A	STARLINK-4691	US	539	541	53.2	53	0	4
2022-105A	STARLINK-4622	US	562	565	97.7	45	0	4
2022-106A	YAOGAN-33 02	PRC	695	697	98.2	0	1	0
2022-107A	STARLINK-4725	US	348	352	53.2	51	0	5
2022-108A	CENTISPACE-1 S3	PRC	691	707	53.5	0	1	0
2022-108B	CENTISPACE-1 S4	PRC	692	708	53.5			
2022-109A	YAOGAN-35 05A	PRC	492	502	35.0	0	1	1
2022-109B	YAOGAN-35 05B	PRC	490	503	35.0			
2022-109D	YAOGAN-35 05C	PRC	492	501	35.0			
2022-110A	EUTE KONNECT VHTS	EUTE	EN ROUTE TO GEO			0	1	0
2022-111A	STARLINK-4718	US	539	541	53.2	34	0	5
2022-112A	CHINASAT 1E	PRC	35777	35797	1.4	0	1	0
2022-113A	STRIX-1	JPN	557	576	97.7	0	2	0
2022-114A	STARLINK-4749	US	390	392	53.2	53	0	4
2022-115A	YUNHAI-1 03	PRC	781	783	98.5	0	1	0
2022-116A	SOYUZ MS-22	CIS	413	422	51.6	0	1	0
2022-117A	USA 338	US	NO ELEMS. AVAILABLE			0	0	0
2022-118A	OBJECT A	PRC	485	508	97.5	0		
2022-118B	OBJECT B	PRC	484	503	97.5			
2022-118C	OBJECT C	PRC	297	660	97.5			
2022-119A	STARLINK-5028	US	348	351	53.2	51	0	4
2022-120A	YAOGAN-36 01A	PRC	493	499	35.0	0	1	1
2022-120D	YAOGAN-36 01B	PRC	491	502	35.0			
2022-120E	YAOGAN-36 01C	PRC	492	501	35.0			